

## Microstructure and Dielectric Properties of Mn Substituted $\text{Sr}_2\text{Cu}_2\text{Fe}_{12}\text{O}_{22}$ ( $\text{Cu}_2\text{Y}$ ) Hexaferrite Powder

Rajshree B. Jotania\*, Pratiksha A. Patel\*\*

\*(Department of Physics, University School of sciences, Gujarat University, Navrangpura, Ahmedabad 380 009, Gujarat, India)

\*\* (Samarth College of Engineering & Technology, Himmatnagar 383 001, Gujarat, India)

### ABSTRACT

Hexaferrites are relatively low cost, chemically stable material and they have found wide range of technological applications in transformer core, high-quality filters, electronic, microwave devices and components. Among all hexaferrites, Y-type hexaferrite is an important type of magnetic materials in VHF and UHF and has gained much interest in recent years due to their multiferroic properties. In this paper we report the microstructural and dielectric properties of the polycrystalline bulk samples of  $\text{Sr}_2\text{Cu}_{2-x}\text{Mn}_x\text{Fe}_{12}\text{O}_{22}$  ( $x = 0.0, 0.6, 0.8, 1.0$ ) hexaferrite prepared by using a chemical co-precipitation synthesis. All hexaferrite samples were characterized using XRD, FTIR, SEM and dielectric measurements. X-ray results confirm that Mn substitution for Cu does not affect the Y-type hexaferrite phase formation. Dielectric measurements were carried out at room temperature in frequency range of  $10^2$  Hz to  $2 \times 10^6$  Hz.

**Keywords** - Y-type hexaferrite, co-precipitation technique, XRD, SEM, Dielectric properties

### I. INTRODUCTION

Hexagonal ferrites are classified on the basis of their chemical composition and crystal structure. They are subdivided into six types: M-type ( $\text{AFe}_{12}\text{O}_{19}$ ), W-type ( $\text{AMe}_2\text{Fe}_{16}\text{O}_{27}$ ), X-type ( $\text{A}_2\text{Me}_2\text{Fe}_{28}\text{O}_{46}$ ), Y-type ( $\text{A}_2\text{Me}_2\text{Fe}_{12}\text{O}_{22}$ ), Z-type ( $\text{A}_3\text{Me}_2\text{Fe}_{24}\text{O}_{41}$ ) and U-type ( $\text{A}_4\text{Me}_2\text{Fe}_{36}\text{O}_{60}$ ); where A represents ions like Ba, Sr or Pb, and Me represents divalent metal ions like Mg or Zn. The crystalline and magnetic structures of the different types of hexaferrites are remarkably complex and can be considered as a superposition of T, R and S blocks along the hexagonal c-axis. Where T block of four types of oxygen ions ( $\text{O}_4\text{-BaO}_3\text{-BaO}_3\text{-O}_4$ ) with the composition  $\text{Ba}_2\text{Fe}_8\text{O}_{14}$ , R is a three oxygen layer block ( $\text{O}_4\text{-BaO}_3\text{-O}_4$ ) with the composition  $\text{BaFe}_6\text{O}_{11}$ , S block is a two oxygen layer block ( $\text{O}_4\text{-O}_4$ ) with

composition  $\text{Fe}_6\text{O}_8$  which is also known as spinel block.

The Y-structure can be built up from spinel blocks of two oxygen layers which are connected by a block T, one above the other, two layers with barium ions. The layers containing barium (or strontium or lead) are hexagonal packed with respect to their adjacent oxygen layer. These barium ions are larger than the oxygen ions. Therefore the distance between the oxygen layers which contain no barium ion. The distances are 2.40 and 2.32 Å respectively. The projection of the distance between the centers of the Ba ions on to the axis is 2.90 Å, from which it follows that the centers of the barium ions lies at a distance of 0.25 Å out of the plane of the nearest oxygen layer [1, 2]. The unit cell with hexagonal symmetry (space group  $R\bar{3}m$ ) consists of 18 oxygen layers with a repeat distance extending through only six oxygen layers. the length of the c axis being 43.56 Å. In the hexagonal element cell each layer again contain four large ions. There are four successive layers of four oxygen ions, followed by two layers each containing three oxygen ions and one barium ion. The unit cell is composed of the sequence STSTST including three formula units. The metallic cations are distributed among six sublattices as shown in table 1. Three octahedral ions of sublattices  $6c_{VI}$  and  $3b_{VI}$  lies on a vertical threefold axis while the central  $3b_{VI}$ , ion sharing two faces of its coordination with the adjacent  $6c_{VI}$  ions inside T block. Such a configuration possesses a higher potential energy of the structure due to a stronger electrostatic repulsion between the cations; therefore such sites are likely to be preferred by low charge ions. The Y-type hexagonal hexaferrites have gained much interest in recent years due to their multiferroic properties [3-5]. These ferrites are used in electronic communication, microwave devices and components<sup>6</sup>. Miniaturization of ferrite devices in the electronic communication requires high-permeability materials at relatively lower microwave frequencies (0–10 GHz) and Y-type hexaferrite considered as

potential material for technical applications. High permeability in Y-type ferrite is attributed to spin rotation and domain wall motions. Y-type hexaferrite is an important type of soft magnetic materials in VHF and UHF [7-14].

**Table 1.** Number of ions per unit formula, coordination and spin orientation for the various metallic sublattices of Y-structure [15].

Sublattice	Coordination	Block	Number of ions	Spin
6c <sub>IV</sub>	tetrahedral	S	2	Down
3a <sub>VI</sub>	octahedral	S	1	UP
8h <sub>VI</sub>	octahedral	S-T	6	UP
6c <sub>VI</sub>	octahedral	T	2	Down
6c <sub>IV</sub>	tetrahedral	T	2	Down
3b <sub>VI</sub>	octahedral	T	1	UP

The physical properties of Y-type hexaferrite depends on many factors like preparation methods, sintering temperature, time, chemical composition and amount of substitution etc. Many studies have been reported on addition of divalent, trivalent and tetravalent ions in Y-hexaferrites [16-21], but according to our knowledge none has reported Mn substituted Y-type strontium-copper hexaferrite. Our work focuses on the Physical and dielectric studies of Mn doped Y-type hexaferrite prepared. For this purpose Y-type hexaferrite with composition Sr<sub>2</sub>Cu<sub>2-x</sub>Mn<sub>x</sub>Fe<sub>12</sub>O<sub>22</sub> (x = 0.0, 0.6, 0.8 and 1.0) has been prepared using a co-precipitation technique.

## II. EXPERIMENTAL PROCEDURE

### 2.1 Powder preparation

Single-phase hexaferrite powders of Mn doped Cu<sub>2</sub>Y with composition Sr<sub>2</sub>Cu<sub>2-x</sub>Mn<sub>x</sub>Fe<sub>12</sub>O<sub>22</sub> (x = 0.0, 0.6, 0.8, 1.0) were produced by using a co-precipitation technique. A. R. Grade powder of strontium nitrate (Sr(NO<sub>3</sub>)<sub>2</sub>·6H<sub>2</sub>O), ferric nitrate (Fe(NO<sub>3</sub>)<sub>2</sub>·9H<sub>2</sub>O), copper sulfate (CuSO<sub>4</sub>), Manganese nitrate (Mn(NO<sub>3</sub>)<sub>2</sub>·4H<sub>2</sub>O) were used as starting materials. Stoichiometric amount of strontium nitrate, ferric nitrate, copper sulfate and manganese nitrate were mixed in an appropriate amount of de-ionized water. Ammonium solution (30% w/v) was added slowly in the mixture to adjust pH of 8. The mixed solution was stirred for two hours

and was kept at room temperature 24 hours for aging. The obtained precipitates were washed in 1:1 mixture of methanol and acetone followed by 100% de ionized water to remove impurities. The precipitate was dried at 80°C for 24 hours in an oven and then calcined at 950°C for 4 hours followed by furnace cooling to room temperature to get final product of Sr<sub>2</sub>Cu<sub>2-x</sub>Mn<sub>x</sub>Fe<sub>12</sub>O<sub>22</sub> hexaferrite powder.

### 2.2 Characterization

The Fourier transformed infrared spectra (FTIR) of dried precursors and calcinated powder were recorded at room temperature by the KBr pellet method using a FTIR Bruker tensor 27 model. Phase and quantitative analysis were performed by X-ray diffraction using CuKα radiation (λ = 1.5405Å) on PW1830 diffractometer. The 2θ Bragg angles were scanned over a range of 18-90°. Scanning electron micrographs were obtained using a MAKE-LEO/LICA Model STEREOCAN 440 scanning electron microscope. The dielectric properties of Sr<sub>2</sub>Cu<sub>2-x</sub>Mn<sub>x</sub>Fe<sub>12</sub>O<sub>22</sub> (x= 0.0, 0.6, 0.8 and 1.0) samples were investigated using an Agilent Precision LCR meter (Model No. E4980A).

## III RESULTS AND DISCUSSION

### 3.1 FTIR analysis

FTIR spectra of dried precursors and calcinated samples was taken for x = 0.8 and 1.0 samples in order to monitor the structural changes during the synthesis process.

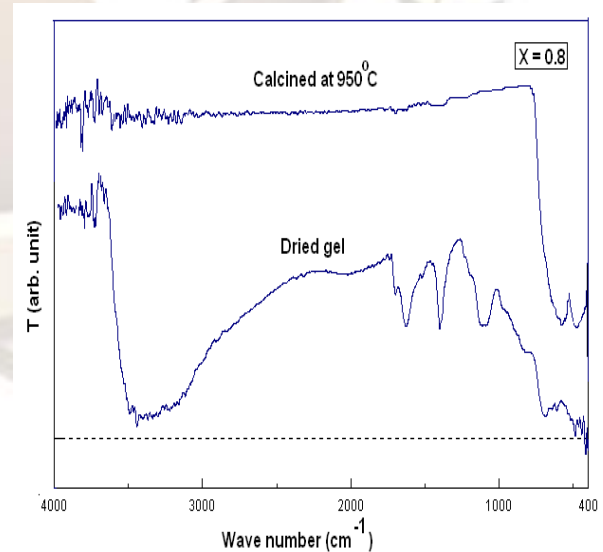


**Fig. 1(a)** FTIR Spectra of Sr<sub>2</sub>Cu<sub>2-x</sub>Mn<sub>x</sub>Fe<sub>12</sub>O<sub>22</sub> (x=0.8) hexaferrite sample

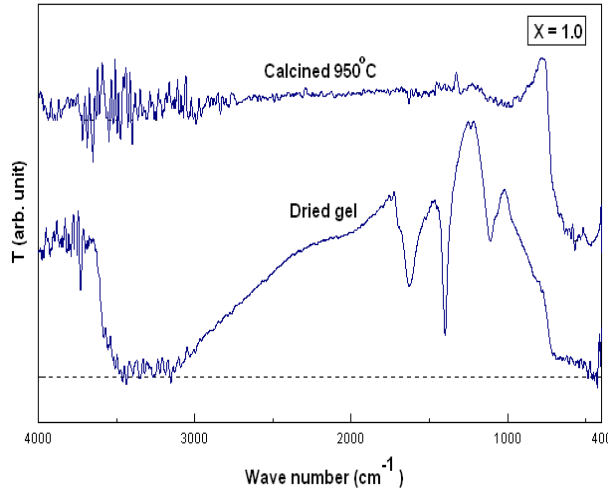


**Fig. 1(b)** FTIR Spectra of  $\text{Sr}_2\text{Cu}_{2-x}\text{Mn}_x\text{Fe}_{12}\text{O}_{22}$  ( $x=1.0$ ) hexaferrite sample

Figure 1 shows the FTIR spectra of as prepared precipitates and the calcinated samples in the wave number range from  $4000\text{ cm}^{-1}$  to  $400\text{ cm}^{-1}$ . Figure 1 (a, b) shows FTIR spectra of dried precursors (heated at  $40^\circ\text{C}$  for 24 hrs) and  $\text{Sr}_2\text{Cu}_{2-x}\text{Mn}_x\text{Fe}_{12}\text{O}_{22}$  ( $x = 0.8$  and  $1.0$ ) hexaferrite particles calcinated at  $950^\circ\text{C}$ , respectively. The spectra of dried precursors indicates the characteristic bands in the range  $3200\text{--}3600\text{ cm}^{-1}$  assigned to O-H stretching vibration of water molecules, while the asymmetrical and symmetrical vibration bands of  $\text{CO}_3^{2-}$  are located around  $1600\text{ cm}^{-1}$ . The bands about  $1380\text{ cm}^{-1}$  are ascribed to the N-O stretching vibration of  $\text{NO}_3^-$ . FTIR results show that after calcination the absorption bands related to O-H,  $\text{CO}_3^{2-}$ , and N-O are disappear. The bands appearing around  $550\text{ cm}^{-1}$  and  $440\text{ cm}^{-1}$  are attributed to M-O stretching vibration of hexaferrite [22-24].

### 3.2 X-ray analysis

Figure 2 (a, b) shows experimental X-ray diffraction patterns for  $\text{Sr}_2\text{Cu}_{2-x}\text{Mn}_x\text{Fe}_{12}\text{O}_{22}$  ( $x = 0.0, 0.6, 0.8$  and  $1.0$ ) samples and a standard pattern for Y-type hexaferrite respectively. All XRD reflection peaks are indexed by applying a hexagonal crystal system and space group  $\text{P6}_3/\text{mmc}$  (here planes [0012], [113], [110], [1013], [116], [119], [024], [0210] [300], [2113], [1025], [220], [3015] used for prepared samples). Lattice constants  $a$  and  $c$  of Mn doped strontium copper hexaferrite samples were calculated using equation (1)

$$\frac{1}{d_{hkl}^2} = \frac{4}{3} \frac{(h^2 + hk + k^2)}{a^2} + \frac{l^2}{c^2} \quad (1)$$

Where  $h, k, l$  are miller indices and  $d$  is inter planer distance. type

The unit cell volume  $V$  of hexagonal crystal is obtained from equation (2)

$$\text{Unit cell volume, } V = \frac{\sqrt{3}}{2} a^2 c \quad (2)$$

The value of lattice constants and cell volume of prepared hexaferrite samples are listed in table 1. From the XRD results, it is evident that mono phase of Strontium Manganese hexaferrite produces at temperature of  $950^\circ\text{C}$ .

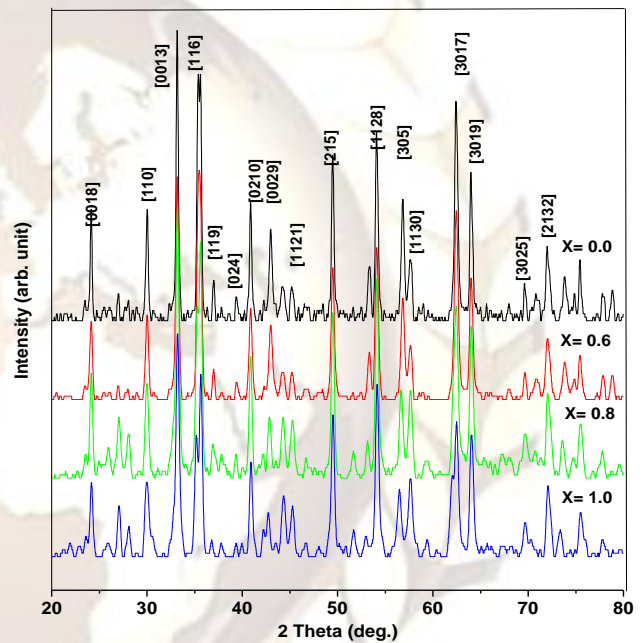


**Fig. 2(a)** XRD diffractogram of  $\text{Sr}_2\text{Cu}_{2-x}\text{Mn}_x\text{Fe}_{12}\text{O}_{22}$  ( $x = 0.0, 0.6, 0.8, 1.0$ ) hexaferrite powder

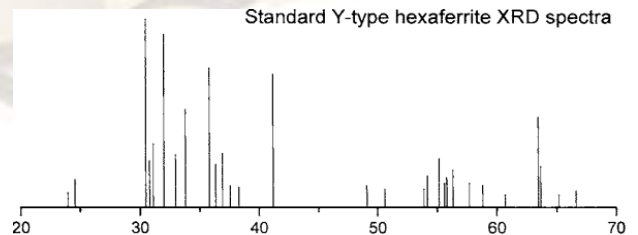


**Fig. 2(b)** Standard XRD pattern of Y- type

**Table 2.** Lattice parameters ( $a$ ,  $c$ ) and cell volume ( $V$ ) of  $\text{Sr}_2\text{Cu}_{2-x}\text{Mn}_x\text{Fe}_{12}\text{O}_{22}$  ( $x = 0.0, 0.6, 0.8$  and  $1.0$ ) samples

Sr. No.	Mn Content ( $x$ )	Lattice constants		
		$a$ (Å)	$c$ (Å)	Volume $V$ (Å <sup>3</sup> )
1	0.0	5.695	59.00	1654.23
2	0.6	5.695	59.02	1657.13
3	0.8	5.695	59.02	1657.13
4	1.0	5.695	59.00	1657.13

The XRD analysis reveals that all samples produce single Y-type phase and there is no effect of Mn substitution on phase formation. The results indicate that the material has a well defined Y-type ferrite crystalline phase. Lattice parameters of all four samples are found almost equal ( $a = 5.690\text{Å}$ ,  $c = 59.00\text{Å}$ ). There is not much effect of Mn substitution on lattice parameters and cell volume because of almost same ionic radii of  $\text{Cu}^{2+}$  ( $0.57\text{Å}$ ) and  $\text{Mn}^{2+}$  ( $0.66\text{Å}$ ).

### 3.3. SEM analysis

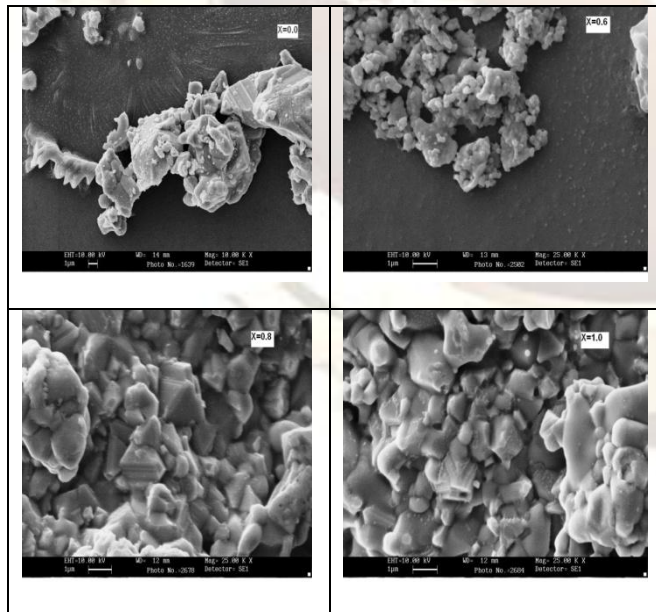


**Fig. 3** SEM micrographs of  $\text{Sr}_2\text{Cu}_{2-x}\text{Mn}_x\text{Fe}_{12}\text{O}_{22}$

Figure. 3 shows SEM micrographs of  $\text{Sr}_2\text{Cu}_{2-x}\text{Mn}_x\text{Fe}_{12}\text{O}_{22}$  ( $x = 0.0, 0.6, 0.8$  and  $1.0$ ) hexaferrite samples sintered at  $950^\circ\text{C}$  for 4 hrs, prepared by a chemical coprecipitation method. It is observed from SEM images that the grains are non-uniform and densely distributed over the surface, more over grain size of the compound is found to be in the range of  $300\text{ nm} - 1.5\mu\text{m}$ . The SEM micrographs show that the grain size of the samples increased distinctly with Mn increases and the porosity decreased.

### 3.4 Dielectric properties

The dielectric measurements were carried out over the frequency range of  $100\text{ Hz}$  to  $2\text{ MHz}$  at room temperature. The variation of dielectric constant (real part,  $\epsilon'$ ) and dielectric loss ( $\tan \delta$ ) with frequency for  $\text{Sr}_2\text{Cu}_{2-x}\text{Mn}_x\text{Fe}_{12}\text{O}_{22}$  ( $x = 0.8, 1.0$ ) hexaferrite samples are shown in figure 4(a) and figure 4(b) respectively. It is clear from figure 4(a, b); the dielectric constant ( $\epsilon'$ ) as well as dielectric loss tangent ( $\tan \delta$ ) decreases with increasing measuring frequency. This decrease behavior of ( $\epsilon'$ ) and ( $\tan \delta$ ) with log frequency can be explained on the basis of the assumption that the mechanism of the polarization process in ferrites [22, 23].

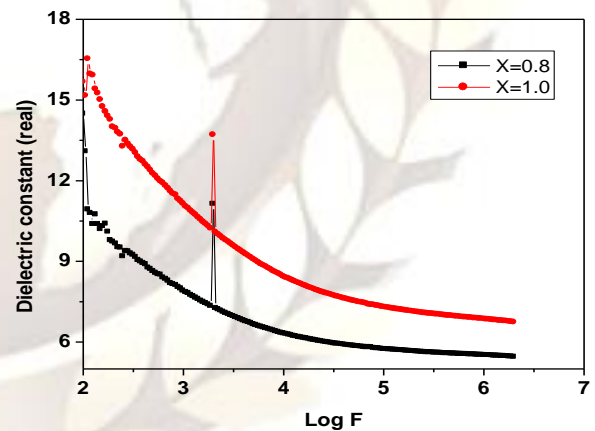


**Fig. 4 (a)** Frequency dependence of dielectric constant (real part,  $\epsilon'$ ) of  $\text{Sr}_2\text{Cu}_{2-x}\text{Mn}_x\text{Fe}_{12}\text{O}_{22}$  ( $x = 0.8, 1.0$ ) hexaferrite samples

The dielectric loss ( $\tan \delta$ ) can be expressed in terms of the real and imaginary parts of the dielectric constant as

$$\tan \delta = \frac{\epsilon''}{\epsilon'} \quad (3)$$

Where  $\epsilon'$  and  $\epsilon''$  are the real and imaginary parts of the dielectric constant respectively

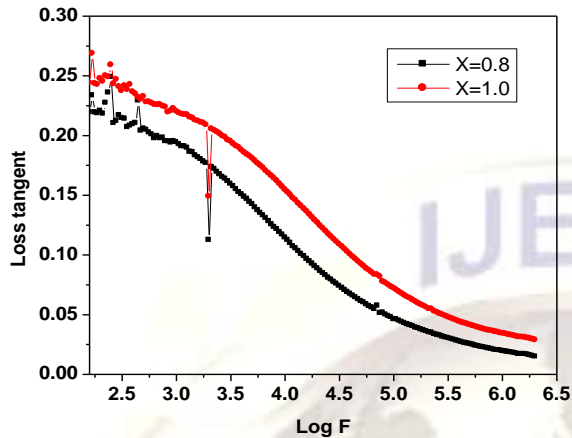


Fig. 4 (b) The variation of dielectric loss tangent with log frequency

#### IV. CONCLUSION

Mn doped  $\text{Cu}_2\text{Y}$  hexaferrite powder ( $\text{Sr}_2\text{Cu}_{2-x}\text{Mn}_x\text{Fe}_{12}\text{O}_{22}$ ) have been synthesized using a chemical co-precipitation synthesis technique followed by a single-step sintering at  $950^\circ\text{C}$  for 4 hrs. Prepared hexaferrite materials were characterized for structure, morphology, and dielectric properties. FTIR results confirm the formation of pure hexaferrite and structural changes produced after calcination at high temperatures. XRD result reveals that Mn doping ( $x = 0.0, 0.6, 0.8$  and  $1.0$ ) does not destroy the phase formation of Y-type hexaferrite. Mn doping increased the grain size and decreased porosity.

#### ACKNOWLEDGEMENTS

The authors are thankful to GUJCOST, Gandhinagar, Gujarat, India for providing partial financial support in the form of minor research project code no.0401121.

#### REFERENCES

[1] M. Y. Salunkhe, D. K. Kulkarni, *J. Magn. Magn. Mater.* 279(1), 2004, 64-68. doi.org/10.1016/j.jmmm.2004.01.046  
 [2] J. Smit, H. P. J. Wijn, *In: Ferrites*, (Philip's Tech Library, New York, 1959)  
 [3] S. Ishiwata, Y. Taguchi, H. Murakawa, Y. Onose, Y. Tokura, *Science* 319,2008,1643-1346.  
 [4] T. Kimura, G. Lawes and A. P. Ramirez, *Phys Rev Lett* 94, 2005,137201-4.  
 [5] S. Ishiwata, Y. Taguchi, Y. Tokunaga, H. Murakawa, Y. Onose and Y. Tokura, *Phy Rev B* 79, 2009, 180408 (R).

[6] Y. Bai, J. Zhou, Z. Gui, L. Li, *Mater Chem Phys* 98(1), 2006, 66-70.  
 [7] M. Obol, X. Zuo, C. Vittoria, *J Appl Phys* 91, 2006, 7616-19. doi:10.1063/1.1446113  
 [8] T.Nakamura, K. I. Hatakeyama, *IEEE Trans Magn* 36,2000, 3415-3417. doi:10.1109/20.908844  
 [9] H. J. Kwon, J. Y. Shin, J. Y. Oh, *J Appl Phys* 75,1994,6109-6111. doi:10.1063/1.355476  
 [10] M. Obol, C. Vittoria, *J Appl Phys* 94,2003, 4013-4017. doi:10.1063/1.1601291  
 [11] M. Obol, C. Vittoria, *IEEE Trans Magn* 39, 2003, 3103-3105. doi:10.1109/TMAG.2003.816019  
 [12] M. Obol, C. Vittoria, *J Magn Magn Mater*, E1799, 2004,272-276. doi:10.1016/j.jmmm.2003.12.1116  
 [13] M. Obol, C. Vittoria, *J Magn Magn Mater* 265,2003, 290-295. doi:10.1016/S0304-8853(03)00277-4.  
 [14] Y. Bai, J. Zhou, Z. Gui, L. Li, *J Magn Magn Mater* 250, 2002, 364- 369.  
 [15] G. Albanese, *Journal de Physique, Colloque CI, supplement au no. 4, Tome 38,1977,CI-85-C194.*  
 [16] G. Albanese, A. Deriu, F. Licci and S. Rinaldi, *IEEE Trans Magn Mag* 14, 1978,710-712.  
 [17] A Deriu, F Licci, S Rinaldi and T Besagni, *J Magn Magn Mater*, 22,1981, 257-260.  
 [18] S. G. Lee and S. J. Kwon, *J Magn Magn Mater*, 153,1996, 279 -284.  
 [19] M. A. El Hiti, and A. M. Abo El Ata, *J Magn Magn Mater* 195,1999, 667-678.  
 [20] Y. Hiraoka, H. Nakamura, M. Soda, Y. Wakabayashi, and T. Kimura, *J Appl Phys*, 110, 2011, 0339201-7.  
 [21] K. Knížek, P. Novák and M. Küpferling, *Phys Rev B* 73,2006,1531031-4.  
 [22] O. Crap, R. Barjeda, E. Segal, M. Brezeanu, *Thermochim Acta*, 318,1998, 57.  
 [23] H. G. Zhang, L. T. Li, Z. W. Ma, J. Zhou, Z. X. Yue, Z. L. Gui, *J Magn Magn Mater* 218, 2000, 67-71.  
 [24] Z. Yue, W. Guo, J. Zhou, Z. Gui, L. Li, *J Magn Magn Mater*, 270, 2004, 216-223.  
 [25] K. W. Wagner, *Amer Phys*, 40,1973, 817-855.  
 [26] C. G. Koops, *Phys Rev*, 83,1951,121-124.